Biophysical Journal, Volume 99

Supporting Material

Residue-specific side-chain packing determines backbone dynamics of transmembrane model helices

Stefan Quint, Simon Widmaier, David Minde, Daniel Hornburg, Dieter Langosch, Christina Scharnagl

Residue-specific side-chain packing determines backbone dynamics of transmembrane model helices

Stefan Quint[#], Simon Widmaier[#], David Minde[#], Daniel Hornburg[#], Dieter Langosch[#], Christina Scharnagl[§*]

[#] Lehrstuhl für Chemie der Biopolymere, Technische Universität München, Weihenstephaner Berg 3, 85354 Freising, and Munich Center for Integrated Protein Science (CIPS[M]), Germany

[§] Fakultät für Physik E14, Technische Universität München, Maximus-von-Imhof-Forum 4, 85354 Freising, Germany

* Corresponding author,
Phone: +49 (0)8161-71-3557, E-mail address: christina.scharnagl@ph.tum.de

Supporting Material

This Supporting Material (3 Tables, 9 Figures) provides details about

1. the correlations between site-specific structural and dynamical properties (Table S1);
2. the comparison of MD derived and experimental DHX kinetics (Table S2, Figs. S1, S2);
3. the convergence analysis of backbone and side-chain fluctuations (Table S3, Figs. S3, S4);
4. additional structural and dynamical properties of LV-peptides (Figs. S5 – S9).

1. Correlation between structural and dynamical properties of LV-peptides

Table S1: Spearman rank order correlation coefficients ρ (1) between site-specific measures for structural and dynamical properties of LV-peptides. [*]

	backbone dynamics	H-bond dynamics		packing	side chain interaction		
	RMSF[$]	$\mathbf{f_\alpha}$ [#]	$\mathbf{k_{DX}}$ [§]	$\mathbf{n_P}$ [π]	$\mathbf{W_{sc\text{-}sc}}$ [‖]	$\mathbf{W_{sc\text{-}bb}}$ [**]	$\mathbf{W_{sc\text{-}all}}$ [##]
RMSF	1	–0.68	0.61	–0.72	–0.54	–0.35	–0.37
$\mathbf{f_\alpha}$		1	–0.92	0.75	0.47	0.44	0.44
$\mathbf{k_{DX}}$			1	–0.66	–0.42	–0.43	–0.44
$\mathbf{n_P}$				1	0.73	0.41	0.49
$\mathbf{W_{sc\text{-}sc}}$					1	0.62	0.63
$\mathbf{W_{sc\text{-}bb}}$						1	0.96
$\mathbf{W_{sc\text{-}all}}$							1

[*] A negative sign of the correlation coefficient indicates inverse proportionality. For each entry 142 site-specific observations have been correlated.

[$] Root mean-square fluctuations of C_α atoms around the mean position.

[#] Probability of α-helical H-bond formation (angle N- H_i ...O_{i-4}: 180°± 60°, distance H_i ...$O_{i-4} \leq 2.6$ Å).

[§] DHX exchange rate. Exchange protection is defined by the presence of carbonyl oxygen atoms at positions i-4, i-5 or i-3 within a distance ≤ 3 Å to the amide proton at position i (see: Methods).

[π] Local packing density defined by the number of noncovalent heavy peptide atoms in a spherical region with radius 7 Å around the amide proton.

[‖] VDW attraction between the side chain of residue i and all other side chains.

[**] VDW attraction between the side chain of residue i and the backbone.

[##] Total interaction of the side chain of residue i with all other side chains and the backbone (includes VDW and electrostatic interactions; note that the electrostatic interaction between side chains in the hydrophobic LV-cores is zero).

2. Comparison of MD-derived and experimental D/H-exchange kinetics of LV-peptides

Table S2: Amide deuteron exchange kinetics calculated from the MD simulations using different descriptions of DHX protection by intramolecular H-bond acceptors.

H-bond acceptor		χ^2_{red} [§]								
type [*]	d_{HO} [#] [Å]	**all** 568 [π]	**L16** 41 [π]	**LLV** 41 [π]	**LV** 41 [π]	**VVL** 41 [π]	**LVL** 101 [π]	**VLV** 101 [π]	**LLVL** 101 [π]	**LVLLV** 101 [π]
α	2.6	4.59	7.06	6.18	2.84	1.80	3.14	5.87	4.79	4.74
α/3_{10}/π	**3.0** [$]	**0.49**	**1.62**	**2.41**	**0.85**	**0.39**	**0.18**	**0.03**	**0.37**	**0.05**
α/3_{10}/π	3.5	3.16	5.77	1.27	2.45	0.48	7.91	1.86	0.41	3.58
α/3_{10}/π	4.0	9.95	7.49	1.04	9.53	0.31	23.6	7.70	9.07	8.06

[*] Included is either the α-helical H-bond (NH_i ...O_{i-4}) only, or additional non-regular H-bonds to O_{i-3} (3_{10}-helical) and O_{i-5} (π-helical).

[#] An intramolecular H-bond is considered as closed, if the H...O distance is below the cutoff d_{HO} and the N-H...O angle is in the range of 180°± 60°.

[§] The quality of the models was assessed by χ^2_{red} (2), the variance of residuals between experimental (3) and calculated deuteron populations $D(t_n)$ for discrete observation times t_n. For each amide, the exchange rate k_{DX} was evaluated from the H-bond population observed in the simulations using the protection criterium given in the first two columns. Using these rate constants, the deuteron population was calculated as superposition of 19 single-exponential decays with D(t=0) = 19.

$$\chi^2_{red} = \sum_{n=1}^{N_{obs}} \frac{\left[D_{exp}(t_n) - D_{calc}(t_n)\right]^2}{\sigma_n^2} \Bigg/ N_{obs}$$

The variance σ_n^2 of the calculated populations is obtained by error propagation from the standard errors of the MD-derived k_{DX} values (compare Fig. S1).

[π] Number of observations N_{obs}.

[$] Cutoff distance used for the final evaluation.

Figure S1: Calculated D/H-exchange rate constants k_{DX}. Dashed lines indicate the borders previously defined to delimit the kinetic subpopulations very fast (vf), fast (f), intermediate (i), and slow (s) (3). Errorbars indicate standard deviations calculated from 10 ns block averages. For B-peptides the parental LLV16 is also included. Val positions are shaded in grey.

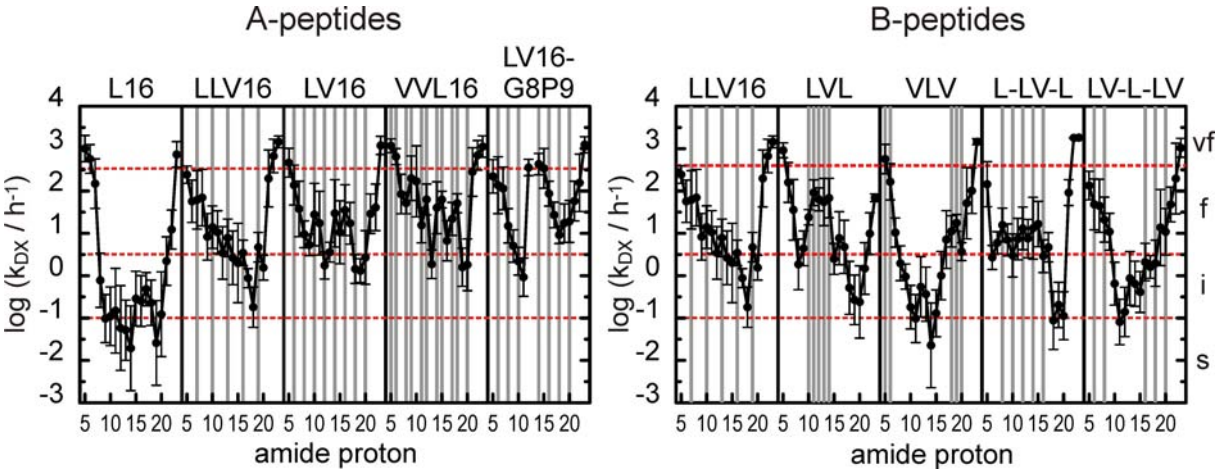

Figure S2: Subclasses of LV-peptides exchanging amide deuterons with rates k_{DX} in different time regimes (compare Fig. S1). The populations obtained from the MD simulations (see Table S2 for parameters) and from the DHX experiments (3) are compared. The borders delimiting the subclasses (Fig. S1) have been varied within ±0.3 around the experimentally defined values to obtain the least deviation. **(*A*)** Sequence-specific population of kinetic subclasses; empty bars refer to experimental values. For the populations from MD, errorbars indicate uncertainities due to the fluctuation of amide deuterons between subclasses (compare the error bars for k_{DX} given in Fig. S1). **(*B*)** Correlation and linear regression for the populations of the four classes (dashed lines) and for all time regimes (black, full line). **(*C*)** Results of the linear regression and Pearson's correlation coefficients r. Note, that over the whole time regime, experimental and calculated populations have a correlation of r = 0.89 and a slope near 1. Slow, intermediate and fast subpopulations are also in very good agreement with the experiments (r = 0.74 to 0.85). Only the very fast population shows less agreement (r = 0.66). The deficient sampling of the conformational space of the termini (compare Fig. S3) and potential experimental errors when determining very fast deuterons (3) may contribute to this discrepancy.

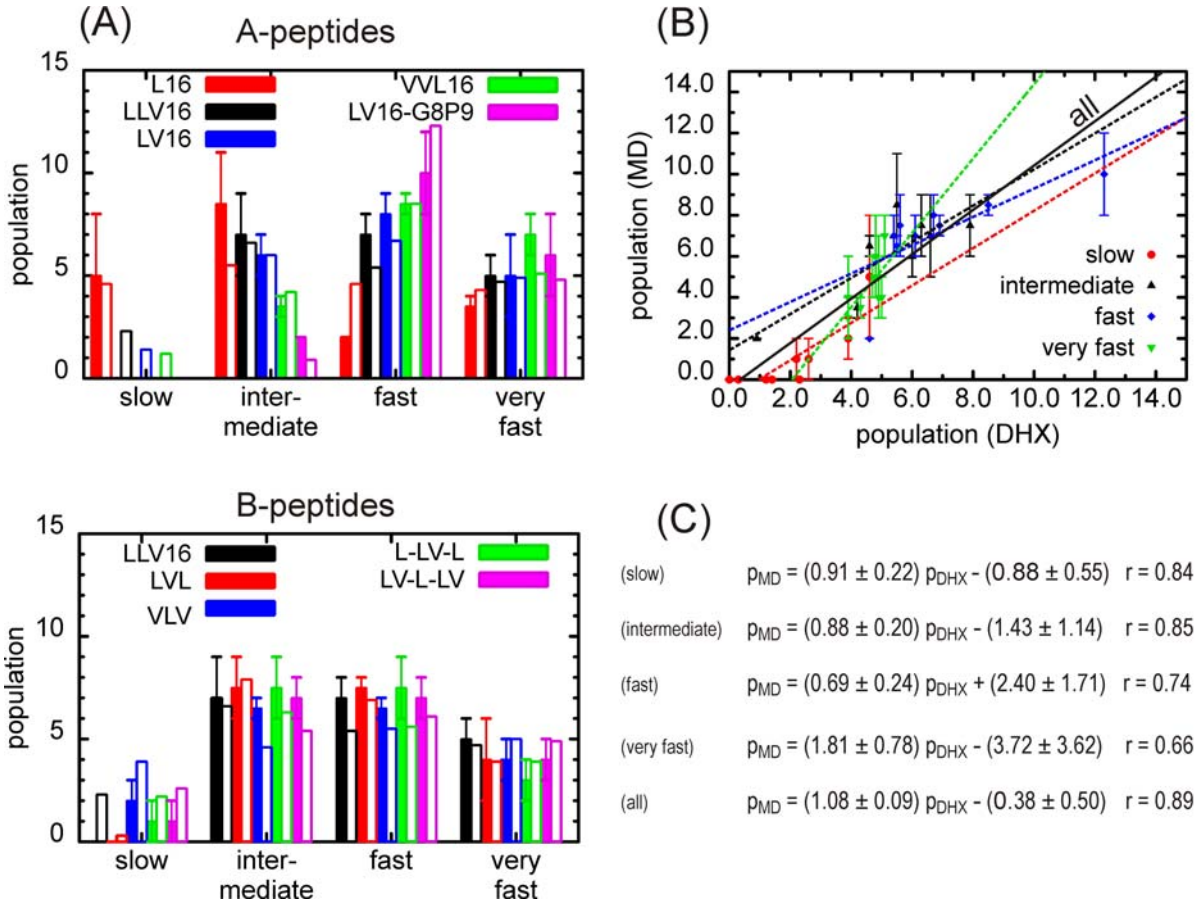

3. Convergence analysis of backbone and side-chain dynamics

Figure S3: Mean distance δ between average structures calculated for time windows of 10 ns and 20 ns, respectively. δ is a measure for convergence of the simulations and should approach 0 Å for a fully converged simulation (4). Rigid body translations and rotations have been removed from the trajectories via a least-square fitting of the backbone to the ideal α-helical starting structures (5,6). A value of $\delta > 1$ Å indicates sampling deficiencies in the frayed terminal regions. For B-peptides the parental LLV16 is also included. Val positions are shaded in grey.

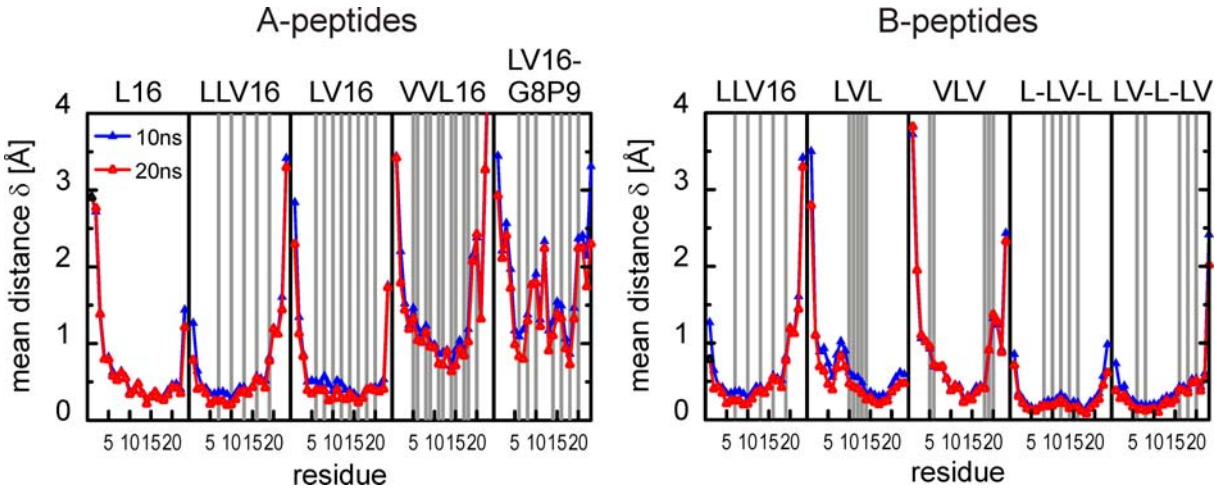

Table S3: **(*A*)** Side-chain and backbone dihedral fluctuations of the hydrophobic core residues of aliphatic A-peptides characterized by the relaxation times τ[ns] of their autocorrelation functions and the population p_t of the *trans* side-chain rotamer (Val positions are shaded in grey).

L16	$\tau_{\chi 1}$ [*,$]	$\tau_{\chi 2}$ [*,$]	p_t [§]	$\tau_{\phi+\psi}$ [#,$]	**LLV16**	$\tau_{\chi 1}$ [*$]	$\tau_{\chi 2}$ [*$]	p_t [§]	$\tau_{\phi+\psi}$ [#,$]
L	0.5	1.0	0.61	6.9	L	1.6	0.5	0.50	1.7
L	0.4	0.8	0.65	0.9	L	1.0	0.4	0.64	0.2
L	0.4	1.1	0.52	0.8	V	2.0		0.80	0.7
L	0.5	1.2	0.62	0.9	L	0.4	0.6	0.60	0.7
L	0.3	1.0	0.53	0.6	L	0.3	1.0	0.71	0.7
L	0.2	0.6	0.53	1.1	V	2.2		0.78	2.4
L	0.4	1.1	0.67	0.9	L	0.2	0.3	0.51	0.7
L	0.5	0.6	0.61	1.2	L	0.2	0.5	0.66	0.7
L	0.3	1.0	0.66	0.9	V	3.8		0.87	1.7
L	1.1	1.4	0.61	0.7	L	0.2	0.3	0.64	1.0
L	0.3	0.5	0.47	1.0	L	1.2	1.6	0.68	0.5
L	0.4	0.6	0.66	0.8	V	2.0		0.97	1.5
L	0.3	0.5	0.50	0.9	L	0.4	0.4	0.52	2.0
L	0.3	0.7	0.58	0.4	L	0.2	0.4	0.58	2.7
L	0.8	1.4	0.66	0.6	V	3.1		0.85	3.3
L	0.4	0.8	0.51	1.4	L	0.5	0.4	0.50	2.0

LV16	$\tau_{\chi 1}$ [*,$]	$\tau_{\chi 2}$ [*]	p_t [§,$]	$\tau_{\phi+\psi}$ [#,$]	**VVL16**	$\tau_{\chi 1}$ [*,$]	$\tau_{\chi 2}$ [*,$]	p_t [§]	$\tau_{\phi+\psi}$ [#,$]
L	0.3	1.6	0.46	1.0	V	2.7		0.53	1.9
V	2.2		0.89	1.0	V	1.9		0.70	2.4
L	0.3	0.6	0.51	0.5	L	1.4	0.3	0.64	0.5
V	1.5		0.80	1.0	V	1.9		0.81	4.1
L	0.3	0.9	0.57	0.5	V	1.6		0.80	5.1
V [‖]	0.8		0.89	2.3	L	1.4	0.3	0.75	1.3
L	0.3	0.7	0.57	1.4	V	5.4		0.50	1.6
V	3.5		0.70	1.3	V	2.3		0.84	2.0
L [‖]	0.3	0.6	0.57	1.9	L	0.3	0.3	0.74	1.9
V [‖]	4.5		0.92	0.9	V	5.8		0.36	1.2
L	0.6	0.6	0.65	0.8	V	0.9		0.90	1.9
V	1.4		0.77	0.8	L	0.5	0.4	0.66	3.0
L	0.2	0.6	0.60	0.6	V	2.4		0.73	6.7
V	3.8		0.77	0.9	V	2.4		0.92	7.5
L	0.2	0.6	0.55	6.6	L	0.3	1.1	0.49	7.7
V	5.0		0.60	3.9	V	2.9		0.82	1.9

[*] The side-chain dihedrals are defined as χ_1 = (N-C^{α}-C^{β}-$C^{\gamma 1}$) for Val and χ_1 = (N-C^{α}-C^{β}-C^{γ}), χ_2 = (C^{α}-C^{β}-C^{γ}-$C^{\delta 1}$) for Leu, respectively.

[#] Backbone dynamics is characterized by the sum of ϕ and ψ dihedrals.

[§] Population p_t of the χ_1=*trans* rotamer ($\chi_1 = 180° \pm 30°$ (Val) and $\chi_1 = 180° \pm 30°$ / $\chi_2 = 60° \pm 30°$ (Leu, tg^+), respectively).

[$] Relaxation times are the result of a single-exponential fit of the autocorrelation function $C(t) = \langle \chi(t')\chi(t'+t) \rangle \approx a \exp(-t/\tau)$ with $C(t=0) = 1$ for times $t > 10$ ps. The variance of residuals is $<10^{-5}$; the maximum standard error is < 2%.

[‖] Examples of side-chain fluctuations and autocorrelation functions for these residues are shown in Fig. S4.

Table S3: **(*B*)** Relaxation times (mean ± standard deviation) for side-chain and backbone dihedral fluctuations in the cores of aliphatic A-peptides.

	Leu	**Val**	**L16**	**LLV16**	**LV16**	**VVL16**
τ_{χ_1} [ns]	0.5 ± 0.3	2.8 ± 1.4				
τ_{χ_2} [ns]	0.7 ± 0.3					
$\tau_{\phi+\psi}$ [ns]			0.9 ± 0.2	1.4 ± 0.3	1.6 ± 1.5	3.2 ± 2.2

.

Figure S4: Side-chain dihedral fluctuations and autocorrelation functions exemplified for three residues of the LV16-peptide. For correlation functions, full lines indicate the result of a single-exponential fit (compare Table S3 *A*). **(*A*)** Leu at position 13. Leu 13 populates mainly two rotamers (58% tg^+, $\chi_1 \sim 180°$, $\chi_2 \sim 60°$; 40% g^-t, $\chi_1 \sim -60°$, $\chi_2 \sim 180°$). Populations of tt ($\chi_1 \sim 180°$, $\chi_2 \sim 180°$) and tg^- ($\chi_1 \sim 180°$, $\chi_2 \sim -60°$) remain <1%. Note that the jump of χ_2 from g^+ to t occurs correlated with the rotation of χ_1 from t to g^-. There are ~330 transitions from the tg^+ rotamers. **(*B*)** Val at positions 10 and 14. The rotamer population for Val 10 is 89% *trans* ($\chi_1 \sim 180°$) and 11% *gauche*+ ($\chi_1 \sim 60°$); Val 14 jumps occassionally also to the *gauche*$^-$ state (92 % t, 4 % g^+, 4 % g^-). For both Val side chains, the number of jumps is ~50.

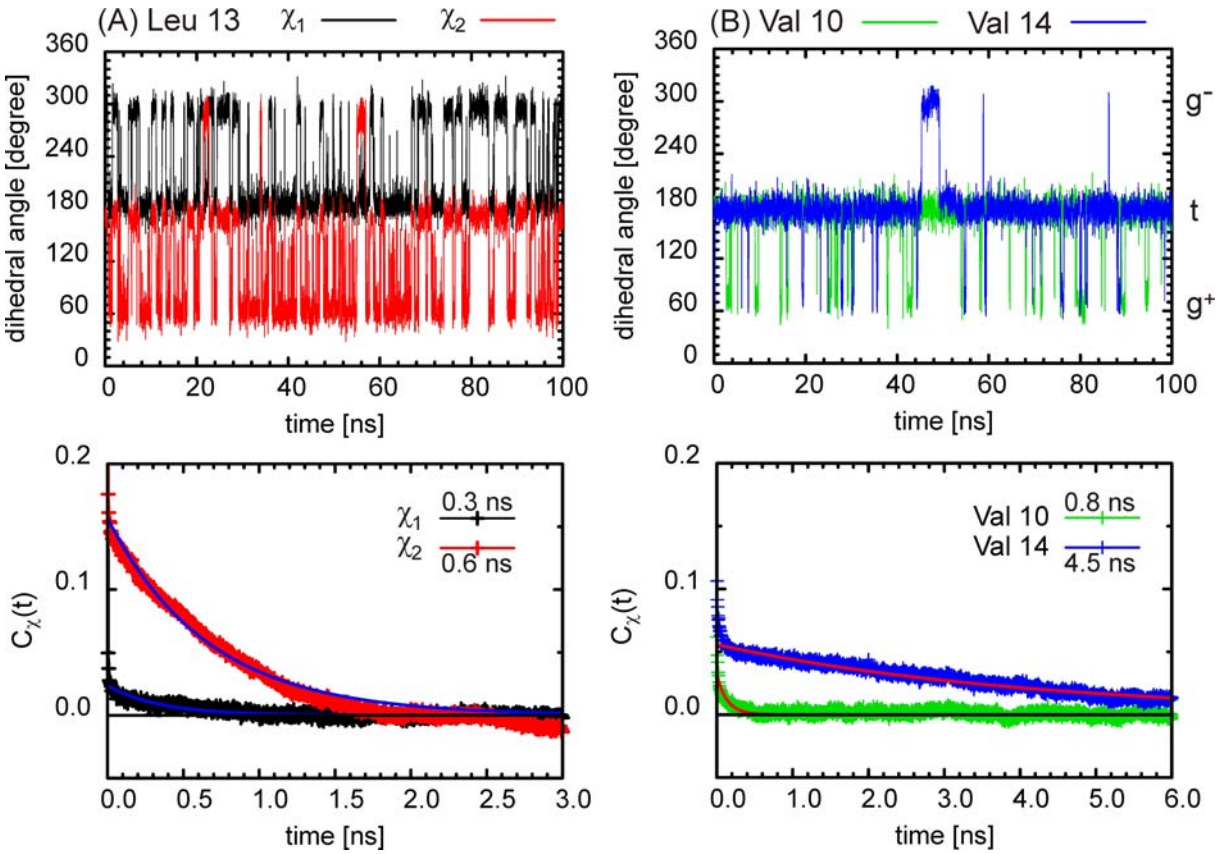

4. Additional information about structural and dynamial properties of LV-peptides

Figure S5: Sequence- and residue-specific structural and dynamical variations of LV-peptides of type B. Errorbars indicate standard errors calculated from 10 ns block averages. Val positions are shaded in grey. The results for the A-peptides are shown in Fig. 1. **(*A*)** C_α-RMSD from an ideal α-helix. Overall rotations and translations were eliminated by a rigid-body fit to the reference structure (5,6). **(*B*)** Population of α-helical and 3_{10}-helical H-bonds. In less than 5% of the trajectories, the amide protons form bifurcated H-bonds.

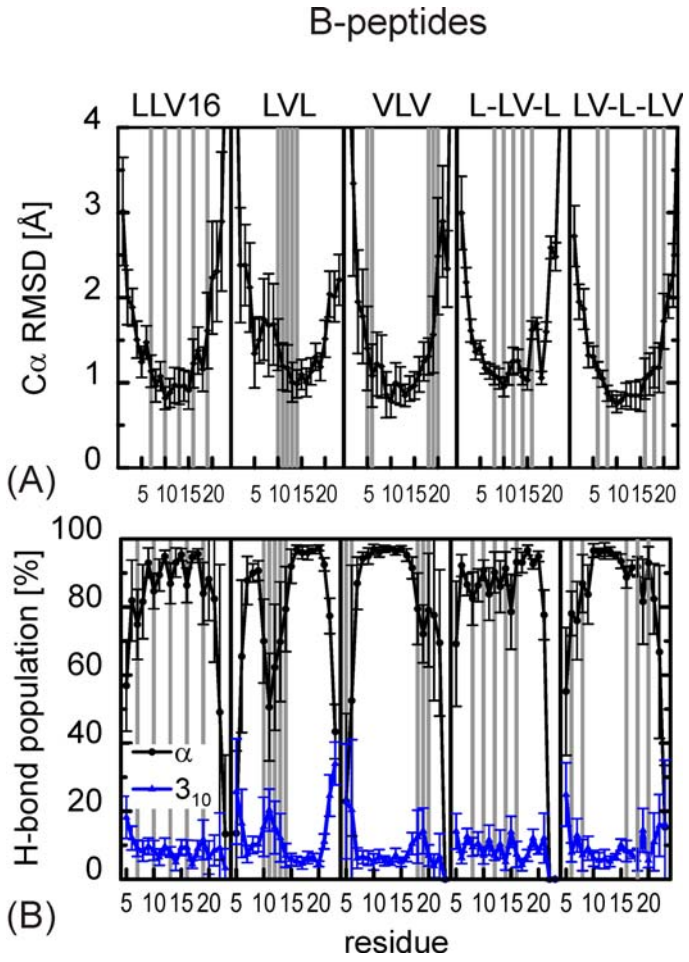

Figure S6: Sequence- and residue-specific side-chain packing of LV-peptides of type B. Val positions are shaded in grey. The results for the A-peptides are shown in Fig. 3. **(*A*)** Contact densities n_P defined by the number of noncovalent heavy peptide atoms in a spherical region with radius 7 Å around the amide protons. The solvent coordination numbers in the same volume are given in Fig. S7. **(*B*)** VDW interaction $W_{sc\text{-}sc}$ between the side chain as position i and all other side chains. The side chain to backbone VDW interactions are shown in Fig. S8.

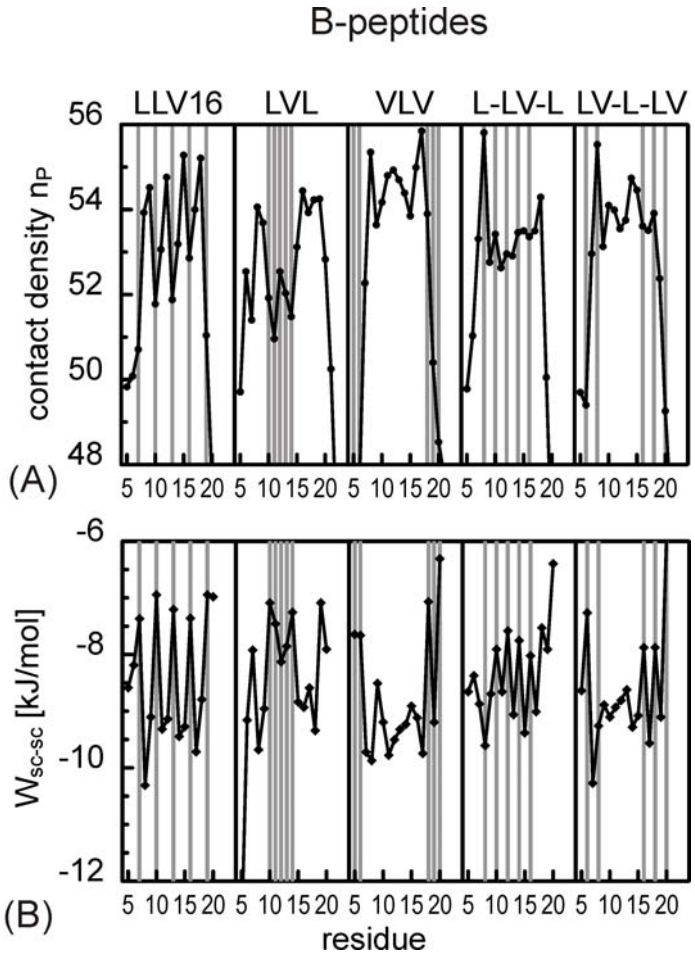

Figure S7: Sequence- and site-specific solvent coordination of LV-peptides. For B-peptides the parental LLV16 is also included. Val positions are shaded in grey. Given are the numbers of water (n_W) and TFE molecules (n_{TFE}) in a sphere with 7 Å around the amide protons. A solvent molecule is counted if its oxygen atom lies within the cutoff distance. The coordination numbers of water and TFE molecules around the amide protons of hydrophobic core residues vary between 2 and 4 without preferential accumulation of water or TFE. A comparable volume of bulk solvent (80%TFE v/v) contains 10 water molecules and 10 TFE molecules, indicating that water and TFE densities are decreased at the LV-cores. Terminal regions are well hydrated with the number density of water molecules approaching its bulk value. TFE is partially excluded at the termini as it reaches only 50% of its bulk value.

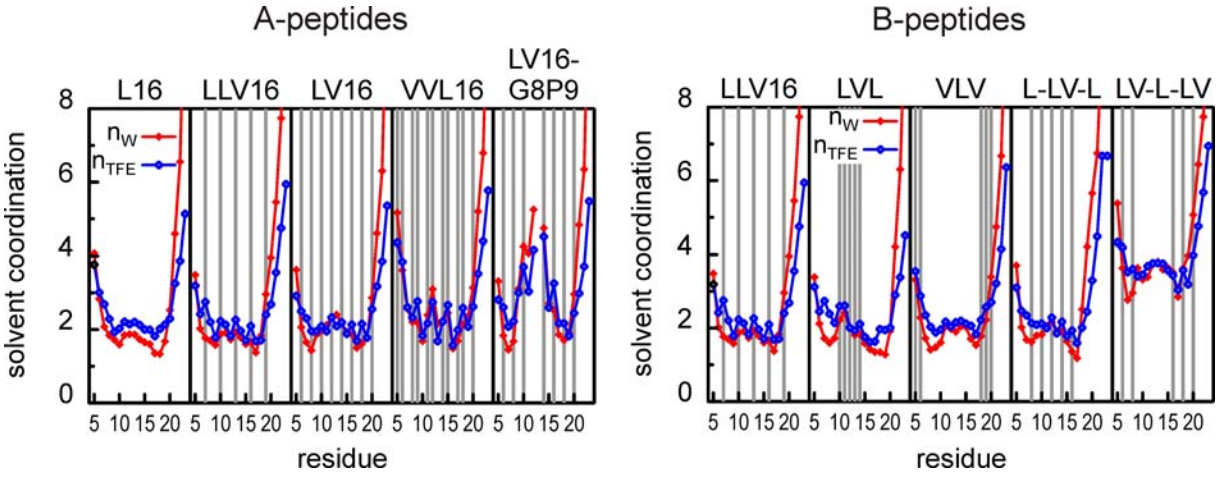

Figure S8: Sequence- and site-specific VDW interactions $W_{sc\text{-}bb}$ between side chains and backbone. For B-peptides the parental LLV16 is also included. Val positions are shaded in grey. The side chain to side chain interactions are shown in Figs. 3 *B* and S6 *B*. The average per-atom VDW attraction between Leu and the backbone ist ~2.8 kJ/mol, for Val it is reduced to ~1.7 kJ/mol.

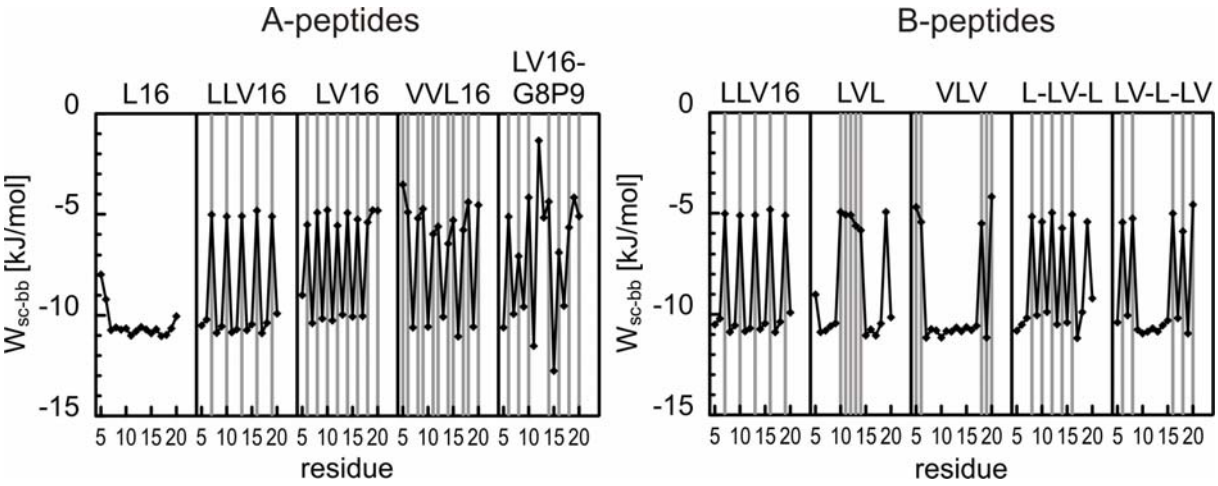

Figure S9: Type and strength of residue-specific VDW interactions in aliphathic A-peptides. The interactions are ordered according to N-terminal (red) and C-terminal contacts (blue). Due to the directionality of the amide H-bond toward the N-terminus, the N-terminal contacts will be more efficient for protection of the amide hydrogen. The sum of the VDW interaction of the individual side chains with all other side chains is shown in Fig. 3 *B*.

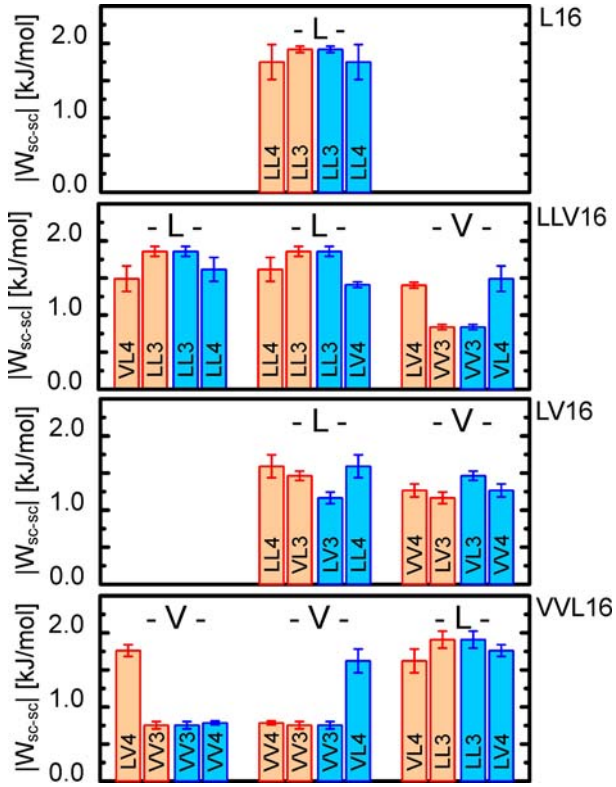

Specifically, the backbone rigidity of L16 can be related to the strong LL3 and LL4 interactions. The pattern of the Leu residues in LLV16 is comparable to L16 leading to comparable helicity and C_α-RMSD. Substitution of Leu by Val in LLV16 replaces the strong LL3 type with the weak VV3 type and leads to local loosening of the structure at the Val-sites. The enhanced dynamics in LV16 can be traced back to the additional weakening of Leu interactions since its strong LL3 contact in LLV16 and L16 is replaced with the weaker VL3 contact in LV16. Another example of striking sequence-specifity concerns the neighboring Val-residues. The unfavorable VV3 contact and the reduction of the VV4 interaction as compared to LV16 both contribute to the large destabilization of adjacent Val residues in VVL16.

REFERENCES

1. Press, W. H.; B. P. Flannery; S. A. Teukolsky, and W. T. Vetterling, editors. 1989. Numerical recipes. The art of scientific computing. Cambridge Univ. Press, Cambridge.
2. Bevington, P. R. 1969. Data reduction and error analysis for the physical sciences. McGraw-Hill, New York.
3. Poschner, B. C., Quint, S., Hofmann, M. W., and Langosch, D. 2009. Sequence-specific conformational dynamics of model transmembrane domains determines their membrane fusogenic function. *J. Mol. Biol.*, 386:733–741.
4. Faraldo-Gómez, J. D., Forrest, L. R., Baaden, M., Bond, P. J. and Domene, C. et al. 2004. Conformational sampling and dynamics of membrane proteins from 10-nanosecond computer simulations. *Proteins: Struct., Funct., Genet.*, 57:783–791.
5. Kabsch, W. 1977. A solution for the best rotation to relate two sets of vectors. *Acta Crystallog. sect. A*, 32:922–923.
6. Kabsch, W. 1978. A discussion of the solution for the best rotation to relate two sets of vectors. *Acta Crystallog. sect. A*, 34:922–923.